THE JOURNAL OF PHYSICAL CHEMISTRY LETTERS
A JOURNAL OF THE AMERICAN CHEMICAL SOCIETY

pubs.acs.org/JPCL

Letter

Kasha's Rule and Koopmans' Correlations for Electron Tunnelling through Repulsive Coulomb Barriers in a Polyanion

Jemma A. Gibbard* and Jan R. R. Verlet*

Cite This: *J. Phys. Chem. Lett.* 2022, 13, 7797−7801

Read Online

ACCESS | Metrics & More | Article Recommendations

ABSTRACT: The long-range electronic structure of polyanions is defined by the repulsive Coulomb barrier (RCB). Excited states can decay by resonant electron tunnelling through RCBs, but such decay has not been observed for electronically excited states other than the first excited state, suggesting a Kasha-type rule for resonant electron tunnelling. Using action spectroscopy, photoelectron imaging, and computational chemistry, we show that the fluorescein dianion, Fl^{2-}, partially decays through electron tunnelling from the S_2 excited state, thus demonstrating anti-Kasha behavior, and that resonant electron tunnelling adheres to Koopmans' correlations, thus disentangling different channels.

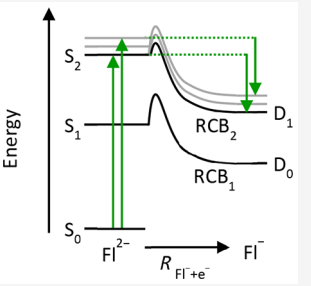

The long-range electronic structure of isolated polyanions is characterized by the repulsive Coloumb barrier (RCB) that arises from the balance of long-range repulsive and short-range attractive forces.[1−5] While often depicted as a single barrier, in reality, the RCB depends on the nuclear and electronic structure of the molecule. There is an RCB associated with each (ro)vibrational level of an electronic state, and each electronic state has its own manifold of RCBs.[6,7] Photoelectron spectroscopy, and in particular, photoelectron imaging, is well-suited to probing RCBs of polyanions.[6−10] Photoelectron spectra are generally characterized by a cutoff in the electron kinetic energy (eKE), below which no photoelectrons are emitted, and therefore offers a direct measure of the ground state RCB height. Resonant electron tunnelling through an RCB reports on the excited state and on the pathway linking the vibrational levels of a polyanion to those of the final state with one less electron.[11−20] Hence, photoelectron spectra of resonant tunnelling give insight into the nature of the excited state RCB. The resonant tunnelling spectra typically show photoelectron emission with an eKE distribution that is independent of photon energy and yields a measure of the energy difference between the mediating resonance and the final state.[11,12] Resonant electron tunnelling through RCBs of the lowest-lying excited states, S_1 and T_1, have been observed.[11−20] Suprisingly, however, tunnelling emission from higher-lying electronic states has, to the best of our knowledge, not been observed, suggesting that there is a Kasha-type rule[21] for electron emission by tunnelling in polyanions. In addition there are questions about the applicability of Koopmans' correlations, which have been used to interpret the photoelecton spectra of excited states, to polyanions.[22,23] Here, we show resonant tunnelling through the RCB of higher-lying electronic states, demonstrating non-Kasha behavior and that the general Koopmans' correlations hold for electron tunnelling.

Among the earliest and clearest examples of resonant tunnelling have been the studies on the doubly deprotonated fluorescein dianion (Fl^{2-}) and the bisdisulizole tetra-anion.[11,12] Both studies showed a photoelectron peak with a fixed eKE distribution that was independent of photon energy. For Fl^{2-}, the photon energy range only covered the $S_1 \leftarrow S_0$ transition,[11] while for bisdisulizole, it covered >4 eV, suggesting multiple excited states were energetically accessible.[12] Kasha's rule pertains to a propensity for fluorescence from the lowest-lying excited state,[21] which can be consolidated by the fact that internal conversion (IC) between close-lying electronic states is typically faster than fluorescence in complex molecules. The photoelectron spectra of bisdisulizole are therefore consistent with an electron tunnelling analogue of Kasha's rule, where photoexcitation to a high-lying excited state is followed by a series of rapid IC processes to the S_1 state, from where the electron ultimately tunnels. The analogous electron tunneling Kasha's rule in polyanions would depend on the competition between IC and electron emission by tunnelling through the RCBs. The latter can be much faster (e.g., ∼1 ps for tunnelling through the S_1 RCB in fluorescein)[11] than fluoresence, raising the general question of whether the resonant electron tunnelling through higher-lying excited state RCBs can occur or whether Kasha's rule is followed.

Received: July 8, 2022
Accepted: August 11, 2022
Published: August 16, 2022

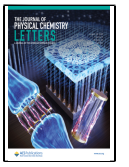

https://doi.org/10.1021/acs.jpclett.2c02145
J. Phys. Chem. Lett. 2022, 13, 7797−7801

We focus on the S_2 state of Fl^{2-} here. The S_1 state has been very well characterized. Fl^{2-} fluoresces strongly in aqueous solution following excitation to S_1 near 500 nm.[24] In contrast, the S_1 state of isolated Fl^{2-} decays by electron emission, which allowed Jockusch and co-workers to record an electronic action (absorption) spectrum of the $S_1 \leftarrow S_0$ transition.[25,26] Additionally, our group has previously perfomed photoelectron imaging following excitation to the S_1 state, which produced a photoelectron spectrum peaking at eKE = 1.64 eV, regardless of the photon energy.[11] We now extend both these studies to probe the S_2 state in the UV spectral range.

Frequency-resolved photoelectron imaging was performed as well as mass-resolved fragment action spectroscopy following irradiation of Fl^{2-} with nanosecond (ns) laser light. The photoelectron imaging apparatus has been described previously elsewhere.[27,28] Modifications have been made to allow the fragment mass and action spectra to be recorded. Fl^{2-} was formed via electrospray ionization of a 5 mM solution of disodium fluorescein salt (Sigma-Aldrich) in methanol. Anions were transferred to a vacuum, and Fl^{2-} was mass-selected using a time-of-flight spectrometer,[29] the temporal focus of which coincided with the interaction region of a velocity map imaging spectrometer,[30] where Fl^{2-} was excited. Tunable UV was produced by a Nd:YAG pumped optical parametric oscillator (OPO). Raw photoelectron images were deconvoluted using the polar onion peeling algorithm,[31] and the resulting photoelectron spectra were calibrated using the spectrum of iodide. Photodetachment of Fl^{2-} also produced the Fl^- anion, which was separated using a reflectron secondary mass spectrometer.[32] The fragment action spectrum was recorded by measuring the yield of Fl^- as a function of the laser wavelength from 300 to 400 nm (UV) and 400 to 600 nm (visible). Supporting electronic structure calculations were performed on both Fl^{2-} and Fl^- using density functional theory (DFT) for ground states and time-dependent DFT with the Tamm−Dancoff approximation for the excited states, at the B3LYP level of theory with the 6-311G ++ 2d,2p basis set.[33,34] The Gaussian 16 software package was used.[35]

Figure 1 shows a Fl^{2-} fragment action spectrum in the range λ = 600−300 nm (2.07−4.13 eV). Note that the dashed line at 400 nm (3.10 eV) highlights different ranges of the light source used, and the relative intensities on either side are not comparable.

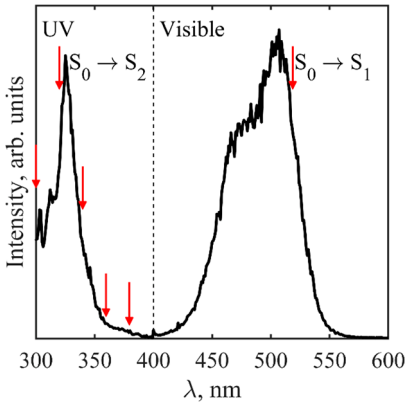

Figure 1. Fl^- fragment action spectrum of Fl^{2-} recorded in the range λ = 300−600 nm. The spectrum below 400 nm (UV), as indicated by a dashed line, has been scaled to a similar intensity as above 400 nm (visible) for clarity. The red arrows indicate the wavelengths where photoelectron images have been acquired.

Figure 1 shows a peak at λ = 507 nm that agrees with previous measurements for the $S_1 \leftarrow S_0$ transition.[25] At λ = 325 nm, a second peak is seen that corresponds to excitation of the $S_2 \leftarrow S_0$ transition.

Figure 2 shows a series of photoelectron spectra of Fl^{2-} recorded in the range spanning the $S_2 \leftarrow S_0$ transition (specific λ

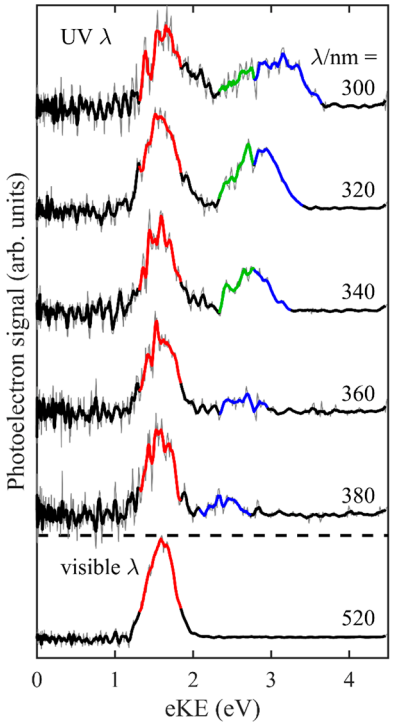

Figure 2. Photoelectron spectra of Fl^{2-} recorded in the range λ = 300−380 nm and at λ = 520 nm. The gray lines are the raw data, and the black lines are a five-point moving average. The red line highlights tunnelling via RCB_1, the green line highlights tunnelling via RCB_2, and the blue line highlights direct detachment over the lowest RCB.

at which the spectra were taken are highlighted with arrows in Figure 1). Additionally, the photoelectron spectrum at λ = 520 nm is shown: this spectrum is representative of *all* spectra taken in the range $460 \leq \lambda \leq 540$, where the excitation is resonant with the $S_1 \leftarrow S_0$ transition.[11] The photoelectron spectra have been plotted in terms of eKE to highlight that certain features are invariant with λ. Three features are observed: (i) a peak centered at a fixed eKE = 1.64 eV (highlighted red); (ii) a rising edge at a fixed eKE = 2.2 eV for $\lambda \leq 340$ nm (highlighted green); and (iii) a peak that shifts to higher eKE with $h\nu$ (i.e., fixed electron binding energy, eBE = $h\nu$ − eKE ≈ 0.7 eV, highlighted in blue). The latter corresponds to direct detachment $Fl^{2-}(S_0) + h\nu \rightarrow Fl^-(D_0) + e^-$, which was also observed in our previous study for $400 \leq \lambda \leq 440$ nm.[11] From this feature, a vertical detachment energy (VDE) of ∼0.7 eV and an adiabatic detachment energy (ADE) of ∼0.5 eV can be extracted for Fl^{2-}. The direct detachment process, which leads to the D_0 anion state, is depicted in Figure 3a, and its shape depends on the S_0/D_0 Franck−Condon factors.

The photoelectron spectrum at λ = 520 nm shows the resonant tunnelling through the S_1 state RCB that has been considered previously.[11] With reference to Figure 3b, the eKE of 1.64 eV corresponds approximately the energy gap between S_1 of the dianion and D_0 of the final anion state. As the S_1 state lies 2.45 eV (507 nm transition energy, Figure 1) above S_0, the

https://doi.org/10.1021/acs.jpclett.2c02145
J. Phys. Chem. Lett. 2022, 13, 7797−7801

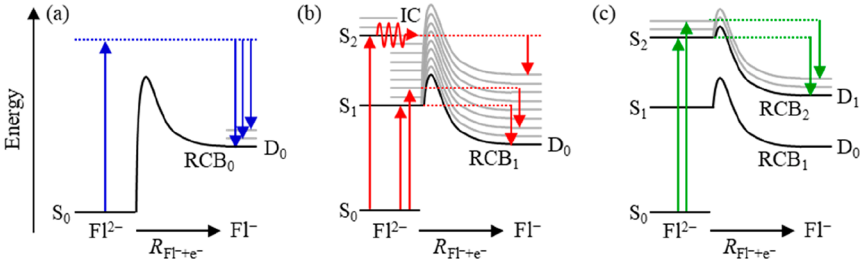

Figure 3. Schematic energy level diagram of Fl^{2-} and Fl^- and relevant photoemission processes. (a) Direct detachment over the lowest energy barrier, RCB_0 (highlighted in blue in Figure 2); (b) tunnelling through RCB_1 from S_1 following excitation to either S_1 directly or to S_2 that subsequently internally converts (IC) to S_1 (highlighted in red in Figure 2); and (c) tunnelling through RCB_2 from S_2 (highlighted in green in Figure 2). Upward arrows indicate excitation and downward arrows electron emission. Dashed lines highlight the energy imparted following excitation. The gray lines indicate vibrational levels with associated RCBs for relevant electronic excited states.

energy of D_0 lies approximately 2.45 − 1.64 = 0.81 eV above S_0, which is consistent with the VDE (~0.7 eV) determined from the direct detachment peak. The feature at eKE = 1.64 eV persists also in the UV spectral range (highlighted in red in Figure 2), where the excitation is resonant with the $S_2 \leftarrow S_0$ transition (see Figure 1). Therefore, at least some population is following Kasha's rule. As shown schematically in Figure 3b, excitation to S_2 can lead to IC to populate S_1 with a large amount of internal energy, and as an electron subsequently tunnels through the S_1 state RCB (RCB_1), internal energy will be conserved in D_0, producing the same eKE spectrum peaking at eKE = 1.64 eV. This Kasha behavior was also observed in the bisdisulizole tetra-anion.[36]

We now turn to the third feature in Figure 2, the low-energy edge to the direct detachment peak, which does not shift with eKE (highlighted in green). This edge does not correspond to a direct detachment cutoff because there is no RCB at this energy for detachment to the D_0 state. If there was, then the direct detachment peak (highlighted in blue) would not be visible in the λ = 380 nm spectrum (or the $400 \leq \lambda \leq 440$ nm spectra shown previously).[11] Instead, we consider the possibility that this feature arises from resonant electron tunnelling through the RCB of the S_2 excited state (RCB_2). The feature peaks approximately at eKE ≈ 2.5 eV (although it is difficult to ascertain exactly because of the spectral overlap with the direct detachment highlighted in blue). The S_2 state lies at 3.82 eV (325 nm from Figure 1), and using a similar energetic argument as for S_1 resonant tunnelling, we find that the final D_n state in the anion lies approximately 3.82 − 2.5 = 1.32 eV above the S_0 state. This is clearly inconsistent with the D_0 state of Fl^-, which we found to be around ~0.8 eV above S_0. However, an excited state in Fl^- following resonant electron tunnelling through RCB_2 could potentially be the final state.

The electronic structures of Fl^{2-} and Fl^- were considered using computational chemistry, with the results summarized in Table 1. All energies for Fl^{2-} are quoted relative to S_0 and are considered as vertical excitations (*i.e.*, in the S_0 geometry). For Fl^-, both vertical and adiabatic energies are quoted, and the D_1 excited state is considered in the D_0 geometry. The calculated transition energies for the S_1 and S_2 states are in reasonable agreement with the fragment action spectrum (Figure 1). Similarly, the calculated VDE is in good accord with that obtained from the photoelectron spectrum (Figure 2). Hence, the calculations have captured the essential electronic structure. On the basis of our proposed resonant tunnelling through RCB_2, we anticipate an excited state of the anion around 1.32 eV, and our calculations indeed show that the D_1 state lies at 1.35 eV. The detachment dynamics can be schematically represented as

Table 1. Calculated Energetics with VDEs and VEEs Calculated using DFT and TD-DFT (TDA) B3LYP/6-311G ++ 2d,2p and Experimental Values Extracted from the Fragment Action Spectrum (Figure 1) and Photoelectron Spectra (Figure 2)[a]

species	calculated vertical energy	experimental energy
Fl^{2-} (S_0)	0	0
Fl^- (D_0)	0.74 (ADE 0.62)	0.7
Fl^- (D_1)	1.35	1.32
Fl^{2-} (S_1)	2.66	2.3
Fl^{2-} (S_2)	3.01	3.6

[a]All energies are relative to S_0 and in electronvolts.

shown in Figure 3c. But why would resonant electron tunnelling from S_2 lead to D_1 rather than D_0?

It is convenient to think of the first excited state as arising from the promotion of an electron from the highest-occupied molecular orbital (HOMO) to the lowest-unoccupied molecular orbital (LUMO) and subsequent excited states to promotion to successively higher-lying LUMOs (e.g., LUMO+1, LUMO+2, etc.). In a Koopmans' picture,[37] this would form the same anion state from Fl^{2-} whether tunnelling occurred via RCB_1 or RCB_2. However, higher-lying states often have mixed character, including core-excited character. To assess this possibility, we considered the electron configurations of the relevant electronic states in terms of the relevant molecular orbitals of Fl^{2-}: HOMO, HOMO−1, LUMO, and LUMO+1 (labeled henceforth as **1**, **2**, **3**, and **4** with increasing energy). The results of the calculations indicate that, in a Koopmans' picture, the removal of the electron in the highest-lying MO from the S_0 ($\mathbf{1}^2\,\mathbf{2}^2$) or S_1 (55% $\mathbf{1}^2\,\mathbf{2}^1\,\mathbf{4}^1$ and 45% $\mathbf{1}^2\,\mathbf{2}^1\,\mathbf{3}^1$) states results in the electronic configuration of the D_0 ($\mathbf{1}^2\,\mathbf{2}^1$) state. The S_2 (60% $\mathbf{1}^1\,\mathbf{2}^2\,\mathbf{3}^1$ and 31% $\mathbf{1}^1\,\mathbf{2}^2\,\mathbf{4}^1$) and D_1 states (97% $\mathbf{1}^1\,\mathbf{2}^2$) have predominantly core-excited character, such that electron loss from the S_2 state would result in the D_1 state in a Koopmans' picture. Hence, the calculations fully support our interpretation that the feature in Figure 2, highlighted in green, arises from resonant electron tunnelling through RCB_2, which is associated with the S_2 electronic state.

Finally, additional evidence that two distinct detachment channels contribute to the high eKE feature for $\lambda < 360$ nm can be gained from the electron angular distributions. These are generally quantified by an anisotropy parameter, $-1 \leq \beta_2 \leq +2$, where $\beta_2 < 0, = 0$, and > 0 correspond to emission predominantly perpendicular, isotropic, and parallel to the laser polarization, respectively.[38] Abrupt changes in β_2 are indicative of changes in electronic character of the molecular orbital from which the

https://doi.org/10.1021/acs.jpclett.2c02145
J. Phys. Chem. Lett. 2022, 13, 7797−7801

electron was removed.[28,39,40] Across the high-eKE feature, the green and blue highlighted areas have distinct β_2 parameters. Specifically, the part assigned to tunnelling though RCB_2 (green) has $\beta_2 \sim 0$, while that for direct detachment (blue) has $\beta_2 \sim -0.5$, confirming the two distinct electron loss channels. The tunnelling feature through RCB_1 (red) has $\beta_2 \sim -0.2$, in agreement with the previously reported value.[11]

On the basis of the above, we conclude that resonant electron tunnelling occurs from both the S_1 and the S_2 states. However, why are both pathways accessible at the same photon energy? For both to be present simultaneously, IC from the S_2 to the S_1 state followed by tunnelling through RCB_1 (Figure 3b) must be competitive with electron loss via tunnelling through RCB_2 (Figure 3c). While we were not able to directly measure the tunnelling rate through RCB_2 in real time, the current experiments do provide some clues into the relative time scales of different processes. As anisotropic photoelectron angular distributions indicate tunnelling occurring on a time scale shorter than rotational dephasing,[41] the isotropic RCB_2 tunnelling feature (green) compared to the anisotropic RCB_1 tunnelling feature (red) suggests that resonant tunnelling through RCB_1 may be faster than through RCB_2. In addition, our previous time-resolved measurements on Fl^{2-} found the tunnelling lifetime through RCB_1 to be ~1 ps,[11] which is significantly faster than has been observed in many other systems.[13−17] Therefore, even if tunnelling via RCB_2 is slower than via RCB_1, it may still be relatively fast. It has also been argued that IC from the S_2 state in Fl derivatives may be relatively slow because of the large S_1-S_2 gap (~0.7 eV) and the large differences in the localization of the electron density in both excited states.[26,42] Therefore, given the observation of non-Kasha's rule electron loss, it seems likely that tunnelling through RCB_2 occurs on a similar time scale to IC from S_2 to S_1 and that both processes are slower than tunnelling via RCB_1 (>1 ps).

For the other polyanionic systems where resonant tunnelling has been observed,[13−17] IC will likely outcompete electron emission, resulting in photoelectron emission that appears to adhere to Kasha's rule. This seems to be the case in the bisdisulizole tetra-anion[12] and in the protoporphyrin IX dianion.[20] We also note that Kappes and co-workers have observed competitive electron tunnelling from the lowest singlet, S_1, and triplet, T_1, states in the isolated $Pd^{(II)}$*meso*-tetra(4-sulfonatophenyl)porphyrin tetra-anions.[15] The observation of both S_1 and T_1 electron emission then requires that the rate of intersystem crossing relative to that of tunnelling is competitive. Finally, it should be noted that anti-Kasha's fluorescence in the condensed phase has been observed previously.[42,43]

The overall picture of a single electronic RCB in a polyanion is clearly invalid, and the energetic landscape is not only spatially anisotropic, but it is also highly complex in energy with an RCB for each (ro)vibrational level of each electronic state. Additionally, not every electronic state in the dianion will correlate to the same electronic state in the final anion following removal of an electron, although a Koopmans' picture seems to hold for electron tunnelling. Note that we have solely considered the electronic RCBs and furthermore note that there are also RCBs associated with fragmentation, which will further complicate the picture.[44,45] The multitude of electronic RCBs can stretch many electronvolts above the lowest direct detachment channel. In the present case of Fl^{2-}, we observe non-Kasha rule behavior either because the IC rate from S_2 to S_1 is relatively slow or because the tunnelling through the RCB is relatively fast. Generally, it is the competition between these processes that determines whether Kasha's rule will be followed. On the basis of the observation that in most cases Kasha's rule is followed, resonant electron tunnelling through high-lying excited state RCBs is not necessarily as fast (or at least significantly slower than IC) as one might intuitively expect.

AUTHOR INFORMATION

Corresponding Authors

Jemma A. Gibbard − *Department of Chemistry, Durham University, Durham DH1 3LE, United Kingdom;* orcid.org/0000-0002-4583-8072; Email: jemma.gibbard@durham.ac.uk

Jan R. R. Verlet − *Department of Chemistry, Durham University, Durham DH1 3LE, United Kingdom;* orcid.org/0000-0002-9480-432X; Email: j.r.r.verlet@durham.ac.uk

Complete contact information is available at: https://pubs.acs.org/10.1021/acs.jpclett.2c02145

Notes

The authors declare no competing financial interest.

Data is available from the corresponding authors upon reasonable request.

ACKNOWLEDGMENTS

J.A.G. is thankful for the support of a Ramsay Memorial Fellowship. This work was supported by the EPSRC (EP/V047787/1).

REFERENCES

(1) Scheller, M. K.; Compton, R. N.; Cederbaum, L. S. Gas-Phase Multiply Charged Anions. *Science* **1995**, *270* (5239), 1160−1166.

(2) Dreuw, A.; Cederbaum, L. S. Multiply Charged Anions in the Gas Phase. *Chem. Rev.* **2002**, *102* (1), 181−200.

(3) Kalcher, J.; Sax, A. F. Gas Phase Stabilities of Small Anions: Theory and Experiment in Cooperation. *Chem. Rev.* **1994**, *94* (8), 2291−2318.

(4) Boldyrev, A. I.; Gutowski, M.; Simons, J. Small Multiply Charged Anions as Building Blocks in Chemistry. *Acc. Chem. Res.* **1996**, *29* (10), 497−502.

(5) Simons, J. Molecular Anions. *J. Phys. Chem. A* **2008**, *112* (29), 6401−6511.

(6) Wang, L.-S.; Ding, C.-F.; Wang, X.-B.; Nicholas, J. B. Probing the Potential Barriers and Intramolecular Electrostatic Interactions in Free Doubly Charged Anions. *Phys. Rev. Lett.* **1998**, *81* (13), 2667−2670.

(7) Wang, X.-B.; Ding, C.-F.; Wang, L.-S. Photodetachment Spectroscopy of a Doubly Charged Anion: Direct Observation of the Repulsive Coulomb Barrier. *Phys. Rev. Lett.* **1998**, *81* (16), 3351−3354.

(8) Wang, X.-B.; Wang, L.-S. Photoelectron Spectroscopy of Multiply Charged Anions. *Annu. Rev. Phys. Chem.* **2009**, *60* (1), 105−126.

(9) Verlet, J. R. R.; Horke, D. A.; Chatterley, A. S. Excited states of multiply-charged anions probed by photoelectron imaging: riding the repulsive Coulomb barrier. *Phys. Chem. Chem. Phys.* **2014**, *16* (29), 15043−15052.

(10) Martinez, F.; Iwe, N.; Müller, M.; Raspe, K.; Schweikhard, L.; Tiggesbäumker, J.; Meiwes-Broer, K.-H. Cresting the Coulomb Barrier of Polyanionic Metal Clusters. *Phys. Rev. Lett.* **2021**, *126* (13), 133001.

(11) Horke, D. A.; Chatterley, A. S.; Verlet, J. R. R. Effect of Internal Energy on the Repulsive Coulomb Barrier of Polyanions. *Phys. Rev. Lett.* **2012**, *108* (8), 083003.

(12) Dau, P. D.; Liu, H.-T.; Yang, J.-P.; Winghart, M.-O.; Wolf, T. J. A.; Unterreiner, A.-N.; Weis, P.; Miao, Y.-R.; Ning, C.-G.; Kappes, M. M.; et al. Resonant tunneling through the repulsive Coulomb barrier of a quadruply charged molecular anion. *Phys. Rev. A* **2012**, *85* (6), 064503.

(13) Horke, D. A.; Chatterley, A. S.; Verlet, J. R. R. Influence of the repulsive Coulomb barrier on photoelectron spectra and angular distributions in a resonantly excited dianion. *J. Chem. Phys.* **2013**, *139* (8), 084302.
(14) Winghart, M.-O.; Yang, J.-P.; Kühn, M.; Unterreiner, A.-N.; Wolf, T. J. A.; Dau, P. D.; Liu, H.-T.; Huang, D.-L.; Klopper, W.; Wang, L.-S.; et al. Electron tunneling from electronically excited states of isolated bisdisulizole-derived trianion chromophores following UV absorption. *Phys. Chem. Chem. Phys.* **2013**, *15* (18), 6726.
(15) Jäger, P.; Brendle, K.; Schwarz, U.; Himmelsbach, M.; Armbruster, M. K.; Fink, K.; Weis, P.; Kappes, M. M. Q and Soret Band Photoexcitation of Isolated Palladium Porphyrin Tetraanions Leads to Delayed Emission of Nonthermal Electrons over Microsecond Time Scales. *J. Phys. Chem. Lett.* **2016**, *7* (7), 1167−1172.
(16) Winghart, M.-O.; Yang, J.-P.; Vonderach, M.; Unterreiner, A.-N.; Huang, D.-L.; Wang, L.-S.; Kruppa, S.; Riehn, C.; Kappes, M. M. Time-resolved photoelectron spectroscopy of a dinuclear Pt(II) complex: Tunneling autodetachment from both singlet and triplet excited states of a molecular dianion. *J. Chem. Phys.* **2016**, *144* (5), 054305.
(17) Veenstra, A. P.; Monzel, L.; Baksi, A.; Czekner, J.; Lebedkin, S.; Schneider, E. K.; Pradeep, T.; Unterreiner, A.-N.; Kappes, M. M. Ultrafast Intersystem Crossing in Isolated $Ag_{29}(BDT)_{12}^{3-}$ Probed by Time-Resolved Pump−Probe Photoelectron Spectroscopy. *J. Phys. Chem. Lett.* **2020**, *11* (7), 2675−2681.
(18) Castellani, M. E.; Avagliano, D.; González, L.; Verlet, J. R. R. Site-Specific Photo-oxidation of the Isolated Adenosine-5′-triphosphate Dianion Determined by Photoelectron Imaging. *J. Phys. Chem. Lett.* **2020**, *11* (19), 8195−8201.
(19) Castellani, M. E.; Avagliano, D.; Verlet, J. R. R. Ultrafast Dynamics of the Isolated Adenosine-5′-triphosphate Dianion Probed by Time-Resolved Photoelectron Imaging. *J. Phys. Chem. A* **2021**, *125* (17), 3646−3652.
(20) Gibbard, J. A.; Clarke, C. J.; Verlet, J. R. R. Photoelectron spectroscopy of the protoporphyrin IX dianion. *Phys. Chem. Chem. Phys.* **2021**, *23* (34), 18425−18431.
(21) Kasha, M. Characterization of electronic transitions in complex molecules. *Discuss. Faraday Soc.* **1950**, *9*, 14.
(22) Blanchet, V.; Zgierski, M. Z.; Seideman, T.; Stolow, A. Discerning vibronic molecular dynamics using time-resolved photoelectron spectroscopy. *Nature* **1999**, *401* (6748), 52−54.
(23) Stolow, A.; Bragg, A. E.; Neumark, D. M. Femtosecond Time-Resolved Photoelectron Spectroscopy. *Chem. Rev.* **2004**, *104* (4), 1719−1758.
(24) Earp, A.; Hanson, C. E.; Ralph, P. J.; Brando, V. E.; Allen, S.; Baird, M.; Clementson, L.; Daniel, P.; Dekker, A. G.; Fearns, P. R. C. S.; Parslow, J.; Strutton, P. G.; Thompson, P. A.; Underwood, M.; Weeks, S.; Doblin, M. A. Review of fluorescent standards for calibration of in situ fluorometers: Recommendations applied in coastal and ocean observing programs. *Opt. Express* **2011**, *19* (27), 26768−26782.
(25) McQueen, P. D.; Sagoo, S.; Yao, H.; Jockusch, R. A. On the Intrinsic Photophysics of Fluorescein. *Ang. Chem. Int. Ed.* **2010**, *49* (48), 9193−9196.
(26) Yao, H.; Jockusch, R. A. Fluorescence and Electronic Action Spectroscopy of Mass-Selected Gas-Phase Fluorescein, 2′,7′-Dichlorofluorescein, and 2′,7′-Difluorofluorescein Ions. *J. Phys. Chem. A* **2013**, *117* (6), 1351−1359.
(27) Lecointre, J.; Roberts, G. M.; Horke, D. A.; Verlet, J. R. R. Ultrafast Relaxation Dynamics Observed Through Time-Resolved Photoelectron Angular Distributions. *J. Phys. Chem. A* **2010**, *114* (42), 11216−11224.
(28) Stanley, L. H.; Anstöter, C. S.; Verlet, J. R. R. Resonances of the anthracenyl anion probed by frequency-resolved photoelectron imaging of collision-induced dissociated anthracene carboxylic acid. *Chem. Sci.* **2017**, *8* (4), 3054−3061.
(29) Wiley, W. C.; Mclaren, I. H. Time-of-Flight Mass Spectrometer with Improved Resolution. *Rev. Sci. Instrum.* **1955**, *26* (12), 1150−1157.
(30) Horke, D. A.; Roberts, G. M.; Lecointre, J.; Verlet, J. R. R. Velocity-map imaging at low extraction fields. *Rev. Sci. Instrum.* **2012**, *83* (6), 063101.
(31) Roberts, G. M.; Nixon, J. L.; Lecointre, J.; Wrede, E.; Verlet, J. R. R. Toward real-time charged-particle image reconstruction using polar onion-peeling. *Rev. Sci. Instrum.* **2009**, *80* (5), 053104.
(32) Boesl, U.; Weinkauf, R.; Schlag, E. W. Reflectron time-of-flight mass spectrometry and laser excitation for the analysis of neutrals, ionized molecules and secondary fragments. *Int. J. Mass Spec. and Ion Proc.* **1992**, *112* (2), 121−166.
(33) Hirata, S.; Head-Gordon, M. Time-dependent density functional theory within the Tamm−Dancoff approximation. *Chem. Phys. Lett.* **1999**, *314* (3), 291−299.
(34) Krishnan, R.; Binkley, J. S.; Seeger, R.; Pople, J. A. Self-consistent molecular orbital methods. XX. A basis set for correlated wave functions. *J. Chem. Phys.* **1980**, *72* (1), 650−654.
(35) Frisch, M. J.; Trucks, G. W.; Schlegel, H. B.; Scuseria, G. E.; Robb, M. A.; Cheeseman, J. R.; Scalmani, G.; Barone, V.; Petersson, G. A.; Nakatsuji, H.; Li, X.; Caricato, M.; Marenich, A. V.; Bloino, J.; Janesko, B. G.; Gomperts, R.; Mennucci, B.; Hratchian, H. P.; Ortiz, J. V.; Izmaylov, A. F.; Sonnenberg, J. L.; Williams; Ding, F.; Lipparini, F.; Egidi, F.; Goings, J.; Peng, B.; Petrone, A.; Henderson, T.; Ranasinghe, D.; Zakrzewski, V. G.; Gao, J.; Rega, N.; Zheng, G.; Liang, W.; Hada, M.; Ehara, M.; Toyota, K.; Fukuda, R.; Hasegawa, J.; Ishida, M.; Nakajima, T.; Honda, Y.; Kitao, O.; Nakai, H.; Vreven, T.; Throssell, K.; Montgomery, J. A., Jr.; Peralta, J. E.; Ogliaro, F.; Bearpark, M. J.; Heyd, J. J.; Brothers, E. N.; Kudin, K. N.; Staroverov, V. N.; Keith, T. A.; Kobayashi, R.; Normand, J.; Raghavachari, K.; Rendell, A. P.; Burant, J. C.; Iyengar, S. S.; Tomasi, J.; Cossi, M.; Millam, J. M.; Klene, M.; Adamo, C.; Cammi, R.; Ochterski, J. W.; Martin, R. L.; Morokuma, K.; Farkas, O.; Foresman, J. B.; Fox, D. J. *Gaussian 16*, Rev. C.01; Gaussian, Inc.: Wallingford, CT, 2016.
(36) Osborn, D. L.; Choi, H.; Mordaunt, D. H.; Bise, R. T.; Neumark, D. M.; Rohlfing, C. M. Fast beam photodissociation spectroscopy and dynamics of the vinoxy radical. *J. Chem. Phys.* **1997**, *106* (8), 3049−3066.
(37) Koopmans, T. Über die Zuordnung von Wellenfunktionen und Eigenwerten zu den Einzelnen Elektronen Eines Atoms. *Physica* **1934**, *1* (1), 104−113.
(38) Reid, K. L. Photoelectron Angular Distributions. *Annu. Rev. Phys. Chem.* **2003**, *54* (1), 397−424.
(39) Lietard, A.; Verlet, J. R. R.; Slimak, S.; Jordan, K. D. Temporary Anion Resonances of Pyrene: A 2D Photoelectron Imaging and Computational Study. *J. Phys. Chem. A* **2021**, *125* (32), 7004−7013.
(40) Anstöter, C. S.; Bull, J. N.; Verlet, J. R. R. Ultrafast dynamics of temporary anions probed through the prism of photodetachment. *Int. Rev. Phys. Chem.* **2016**, *35* (4), 509−538.
(41) Horke, D. A.; Chatterley, A. S.; Verlet, J. R. R. Femtosecond Photoelectron Imaging of Aligned Polyanions: Probing Molecular Dynamics through the Electron−Anion Coulomb Repulsion. *J. Phys. Chem. Lett.* **2012**, *3* (7), 834−838.
(42) Shi, L.; Yan, C.; Guo, Z.; Chi, W.; Wei, J.; Liu, W.; Liu, X.; Tian, H.; Zhu, W.-H. De novo strategy with engineering anti-Kasha/Kasha fluorophores enables reliable ratiometric quantification of biomolecules. *Nat. Commun.* **2020**, *11* (1), 793.
(43) Veys, K.; Escudero, D. Anti-Kasha Fluorescence in Molecular Entities: The Central Role of the Electron-Vibrational Coupling. *ChemRxiv*, 2022.
(44) Boxford, W. E.; Pearce, J. K.; Dessent, C. E. H. Ionic fragmentation versus electron detachment in isolated transition metal complex dianions. *Chem. Phys. Lett.* **2004**, *399* (4), 465−470.
(45) Marcum, J. C.; Weber, J. M. Electronic photodissociation spectra and decay pathways of gas-phase $IrBr_6^{2-}$. *J. Chem. Phys.* **2009**, *131* (19), 194309.

https://doi.org/10.1021/acs.jpclett.2c02145
J. Phys. Chem. Lett. 2022, 13, 7797−7801